Inorganic Chemistry

Article

pubs.acs.org/IC

Carbonyl Amine/Schiff Base Ligands in Manganese Complexes: Theoretical Study on the Mechanism, Capability of NO Release

Weili Zheng, Shuixing Wu, Shanshan Zhao, Yun Geng, Junling Jin, Zhongmin Su,* and Qiang Fu*

Institute of Functional Material Chemistry, Faculty of Chemistry, Northeast Normal University, Changchun 130024, Jilin, People's Republic of China

Supporting Information

ABSTRACT: A compound having the capability of releasing NO upon exposure to visible or near-infrared (vis or NIR) light could be a potential candidate for photodynamic therapy (PDT), which is significant for humans. Here, we investigated a series of Mn(II) complexes (**a**−**d**) based on density functional theory (DFT) to illuminate the mechanism of their behavior of releasing NO. Their structural, spectroscopic, and photodissociable properties were calculated by quantum theoretical methods to give a detailed and warranted explanation of the performance of releasing NO. The results indicate that, for **a**−**d**, releasing NO was attributed to the electron transfer from d_{yz}/d_{xz}(Mn) orbitals to π^*(NO) orbitals at the second excited triplet state (T_2). Importantly, we confirmed the finding in the experiment that **d** could release NO upon exposure to the NIR region and, thus, may be a best candidate for PDT in **a**−**d**. Therefore, to take **d** for example, the analyses of the potential energy curves (PECs) of difference states and electron density difference between the T_2 and the ground state (S_0) were performed to further provide evidence of ligand dissociation and release of NO at the T_2 state. Finally, we hope that our discussion can provide assistance to understand the behavior of the release of NO and design novel photodissociable transition metal nitrosyls for PDT applications.

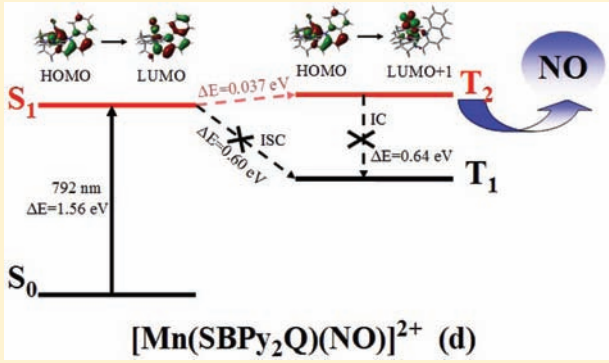

1. INTRODUCTION

Since the discovery of the endogenous nitric oxide (NO) mechanism was proved in 1987, NO has been used in biomedical applications for the vascular smooth muscle relaxation elicited by endothelium-derived relaxing factor (EDRF) and chosen as the "star molecule" in 1992 by *Science*.[1−3] The Nobel Prize for medicine in 1998 was shared by Ignarro, Murad, and Furchgott for their excellent work "NO as gaseous signal molecule of cardiovascular system".[4−6] Further research showed that NO had been used in the fields of regulation of blood pressure, nerve-signal transduction, immune responses, and antimicrobial activity as a biological function molecule.[7−9] Metal nitrosyl complexes,[10−12] as potential candidates for photodynamic therapy (PDT) of cancer cells, have aroused extensive attention since such species can release NO under exposure to certain wavelengths of light.

In recent years, transition metal-based NO donors have been investigated in many experimental works.[13−15] A large number of research works showed that some complexes could release NO upon exposure to near-ultraviolet (NUV) light, which, unfortunately, could be harmful to living cells.[16] For this reason, it would be more meaningful to develop the complex releasing NO upon illumination with light of longer (500−850 nm) wavelengths (visible and near-infrared (vis−NIR) light). This aim can be meet by two strategies: the two-photon excitation technique to active the release of NO[17,18] and designing new metal complexes to work as endogenous NO donors only needing NIR light exposure. The former is not easily achieved because the complex should absorb two photons simultaneously or successively under excitation by ultrafast pulses of laser light. Several research groups selected the latter strategy to release NO from designed complexes.[14,19,20] Early on, the attachment of the electron-rich substituents to the ligand frame might modulate the energy of the $d_\pi(M) \rightarrow \pi^*(M-NO)$ transition and, thus, lead to the maximum absorption of the photoband exhibiting a significant red shift into the low-energy band. For instance, Sellmana et al. reported a new ruthenium complex [Ru(NO)($py^{si}S_4$)]Br containing sterically bulky $SiPh_3$ ligand in an ortho position with regard to the thiolate donors, which could reversibly release NO under vis light (>455 nm) illumination.[14] Additionally, by extending the conjugation of the ligand frame to shift the photoband of metal nitrosyls into vis region, Mascharak et al. have synthesized a diamagnetic {Fe-NO}^{6} nitrosyl $[(PaPy_2Q)Fe(NO)](ClO_4)_2$ derived from the quinoline-based ligand $PaPy_2QH$, in which the quinoline group replaces the pyridine ring of $PaPy_3H$ ligand.[20] Their results show that a quinoline moiety in place of a pyridine had improved the efficiency of NO release under low-intensity vis light (500 nm). Moreover, a new method to synthesize metal

Received: June 3, 2011
Published: March 13, 2012

   dx.doi.org/10.1021/ic2011953 | *Inorg. Chem.* 2012, 51, 3972−3980

nitrosyls releasing NO under vis light via the use of dyes as coordinating ligand has been provided. For example, namely [(Me_2bpb)Ru(NO)(Resf)] and [(Me_2bQb)Ru(NO)(Resf)] ruthenium nitrosyls were synthesized by Mascharak et al.[21,22] The results indicate that the photoactivity of two ruthenium nitrosyls in the vis region (500−510 nm) has been substantially improved by using the red dye resorufin.

Recently, Mascharak et al. have synthesized [Mn($PaPy_3$)(NO)]ClO_4 (**a**), [Mn($PaPy_2Q$)(NO)](ClO_4) (**b**), [Mn($SBPy_3$)(NO)](ClO_4)$_2$ (**c**), and [Mn($SBPy_2Q$)(NO)](ClO_4)$_2$ (**d**) manganese nitrosyls (Figure 1).[23−25] The four complexes

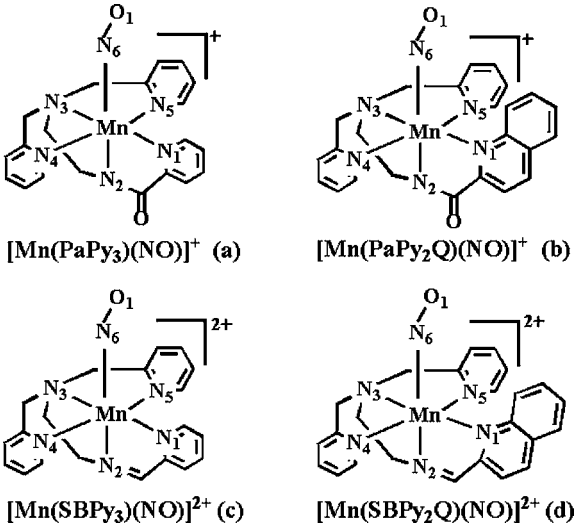

Figure 1. Calculation models of Mn(II) complexes **a**−**d**.

have been proven to have the faculty of releasing NO when they are exposed to vis or NIR light. Especially for **d**, since it is the first metal nitrosyl complex releasing NO rapidly upon exposure to NIR light (900 nm), **d** could be an important candidate for PDT. Up to the present, there are few theoretical studies on the mechanism of NO release behaviors of Mn(II) complexes mainly through analysis of electron transition nature.[26] In this work, we conducted a comprehensive and systematic theoretical study on the mechanism of NO dissociation of the series of Mn nitrosyls. By analysis of the electronic structures and the chemical bond features of Mn−$N_6(O_1)$ in **a**−**d**, the mechanism of NO dissociation was explicitly illustrated. We hope that our work could provide a thorough understanding of the photodissociation mechanism and help for further design of new efficient metal nitrosyls for PDT applications.

2. COMPUTATIONAL DETAILS

The BP86 functional has proven its great predominance in calculation of the structure of transition metals in the ground state (S_0) in the past.[27−34] Thus, the S_0 geometries of the four Mn(II) complexes (Figure 1) were fully optimized without any symmetry constraints by density functional theory (DFT) calculations using the BP86 functional[35,36] with the TZVP basis set applied for the Mn[37] atom and the 6-31g* basis set for all other atoms. The corresponding frequency calculations were performed, on the basis of the optimized S_0 geometries, at the same level of theory to confirm that the optimized geometries were minima on the potential energy surface. On the basis of the optimized S_0 geometries of the complexes, the time-dependent DFT (TDDFT) approach was applied to investigate the electronic properties of singlet and triplet excited states, in which the solvent effect of acetonitrile was taken into account by using the polarizable continuum model (PCM).[38] The chemical bond Mn−$N_6(O_1)$ features for **a**−**d** at S_0 geometries were evaluated by natural bond orbital (NBO),[39] charge decomposition analysis (CDA),[40,41] and Wiberg's bond order analysis. The orbital component and the fragment orbital correlation were analyzed using the Aomix program.[42,43] Electronic distributions of the second triplet excited states (T_2) were visualized using the electron density difference maps (EDDMs) obtained by GaussSum.[44]

For the closed shell systems, the Wiberg bond order indices of the bond between A and B atoms, W_{AB}, were calculated in the NAO^2 [see refs 39 and 45] basis as

$$W_{AB} = \sum_{\mu\in A}\sum_{\nu\in B}(D_{\mu\nu}^{NAO})^2 \quad (1)$$

where μ and ν denote the atom orbitals.

D is the total density matrix:

$$D_{\mu\nu} = 2\sum_{i}^{occ} C_{\mu i}C_{\nu i} \quad (2)$$

where C is the matrix of MO coefficients.

For the linear molecules, the expressions for W_{AB} can be written as

$$\begin{aligned} W_{AB} &= \sum_{\substack{\mu\in A\\ \nu\in B}}\sum_{\substack{\mu\in\sigma\\ \nu\in\sigma}}(P_{\mu\nu}^{NAO})^2 + \sum_{\substack{\mu\in A\\ \nu\in B}}\sum_{\substack{\mu\in\pi\\ \nu\in\pi}}(P_{\mu\nu}^{NAO})^2 \\ &\quad + \sum_{\substack{\mu\in A\\ \nu\in B}}\sum_{\substack{\mu\in\delta\\ \nu\in\delta}}(P_{\mu\nu}^{NAO})^2 \\ &= W_{AB}^{\sigma} + W_{AB}^{\pi} + W_{AB}^{\delta} \end{aligned} \quad (3)$$

where μ and ν denote the atom orbitals, A and B denote the atoms, and P denotes the density matrix.

The magnetic coupling constant (J_{ab}) value was calculated using the following eq 4.[46,47]

$$J_{ab} = \frac{^{LS}E(X) - {}^{HS}E(X)}{^{HS}\langle S^2\rangle - {}^{LS}\langle S^2\rangle} \quad (4)$$

Table 1. Optimized Bond Lengths (Å) for the S_0 of a−d with the Available Experimental Values

	a		b		c		d	
	S_0	exp[23]	S_0	exp[24]	S_0	exp[25]	S_0	exp[25]
Mn−N_1	1.996	1.995	2.057	2.087	1.996	2.007	2.063	2.025
Mn−N_2	1.954	1.955	1.956	1.956	1.986	1.985	1.989	2.092
Mn−N_3	2.062	2.028	2.062	2.066	2.066	2.028	2.069	2.026
Mn−N_4	2.042	2.023	2.064	2.062	2.042	2.014	2.047	2.019
Mn−N_5	2.048	2.034	2.041	2.033	2.053	1.999	2.046	1.979
Mn−N_6	1.666	1.660	1.665	1.678	1.663	1.649	1.661	1.651

dx.doi.org/10.1021/ic2011953 | Inorg. Chem. 2012, 51, 3972−3980

Table 2. Total Energies and Total Spin Angular Momentum for the Singlet (LS) and Triplet (HS) States, the (J_{ab})[a] Value in the Mn−N_6 (2.261 Å) Bond for d Obtained by UBP86 with TZVP/6-31g* Basis Sets, and Spin Density Distributions (SDDs) in Mn−N_6 (2.261 Å) for d at the Singlet State

Mn−N_6/Å	$(E_{LS})^b$	$(E_{HS})^b$	$\langle S^2\rangle_{LS}$	$\langle S^2\rangle_{HS}$	J_{ab}	Mn_{SD}	N_{6SD}
2.261	−2482.8673	−2482.8653	0.9946	2.1722	−372.72	1.294	−0.633

[a] J_{ab} values from eq 4 are shown in inverse centimeters. [b] E_{LS} and E_{HS} are shown in Hartree.

where $^{LS}E(X)$ and $^{HS}E(X)$ denote the total energies in the broken-symmetry (BS) singlet state and triplet state, respectively, and $^{HS}\langle S^2\rangle$ and $^{LS}\langle S^2\rangle$ denote the total spin angular momentum of high-spin state and broken-symmetry singlet state, respectively.

The potential energy curve (PEC) of two dimensions was produced to interpret the photodissociation mechanism of the Mn−N_6(O_1) bond. Here, the *Y* axis represents the relative energy and the *X* axis represents the Mn−N_6 distance. The PECs of the S_0 and the broken-symmetry ground states (S_{0mix}) were determined by optimizing the Mn−N_6 bond distance elongated by the step size of 0.1 Å. For every step, the Mn−N_6 bond was frozen, and the geometry of the complex was relaxed to a stationary point. The PECs of the lowest singlet excited state (S_1) and the lowest and second triplet excited states (T_1 and T_2) were obtained by TDDFT/BP86. Further exploration of the PEC of the T_1 state was carried out using the unrestricted BP86 functional (UBP86). All calculations were performed using Gaussian 09 software package.[48]

3. RESULTS AND DISCUSSION

3.1. Molecular Structures in the Ground State. In order to obtain the good structures for **a**−**d**, the BP86 method was employed to optimize their S_0 structures. The calculated bond lengths for **a**−**d** collected in Table 1 are in good agreement with the corresponding X-ray results, except for the Mn−N_2 bond in **d**. The slight discrepancy in **d** may be caused by optimizing geometry at single molecule level without considering the intermolecular interaction, which clearly affects the geometrical parameters in X-ray data.[49] For **a** and **b**, the Mn−N_2 bond length is shorter than that of **c** and **d** due to the different character of ligand atom N_2. Meanwhile, the trans effect of the N_2 atom would cause the longer bond lengths of Mn−N_6 of **a** and **b** than those of **c** and **d**. The difference of Mn−N bond length in **a**−**d** by the calculation is consistent with the experiment.[25]

3.2. Magnetic Interactions. To confirm the diamagnetism of **a**−**d** at the S_0 state both in solid state and in solution observed by the experimental work, take **d** for example, we employ the broken-symmetry approach with the BP86 functional to evaluate the magnetic coupling constant J_{ab}. The J_{ab} value and the spin density distributions in the elongated Mn−N_6 bond (2.261 Å) for **d** are listed in Table 2. The J_{ab} value indicates that the elongated Mn−N_6 bond (2.261 Å) for **d** possesses the antiferromagnetic property. As shown previously,[50] in the broken-symmetry approach, the spin densities in the singlet state are not strictly related to real spin populations; however, they are still useful in describing the magnitude of electron and spin correlations. The spin densities in the elongated Mn−N_6 bond (2.261 Å) of **d** indicate that the S_0 has the antiferromagnetic property. Such result of magnetic property in **d** is similar to the result of magnetic switching controlled of Nickelate(III) dimers.[51] However, the closed shell and open shell singlet states, based on the normal Mn−N_6 bond (1.661 Å) of **d** in S_0, have the same energy (see the Supporting Information, Table S5). Thus, a strong coupling exists between the Mn(II) centers and unpaired electron of NO in S_0 of **d**, which agrees well with the diamagnetic property of **d** in the experiment.

3.3. Mn−NO Bonding Analysis. In order to investigate the form of the Mn−NO bond for **b** and **d**, NBO and CDA were performed. The diagrams of NBOs for the Mn−NO bond are displayed in Figure 2. Figure 2 shows that the Mn−NO

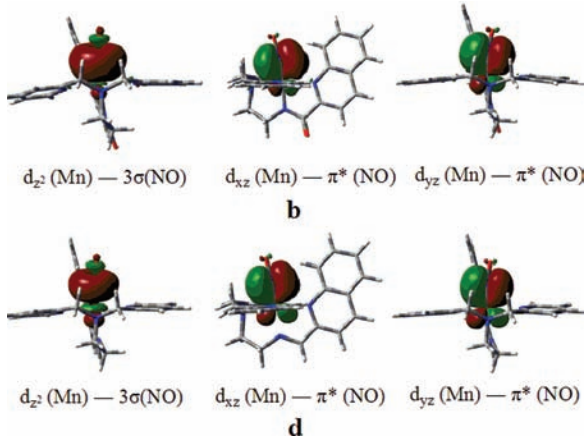

Figure 2. Three forms of NBOs for Mn−NO bond for **b** and **d**.

bond possesses three bonding characters, containing (1) d_{z^2}(Mn)—3σ(NO) (σ-coordination bond), (2) d_{yz}/d_{xz}(Mn)—π*(NO), and (3) d_{xz}/d_{yz}(Mn)—π*(NO). In the later two modes, one is the π back-donating bond, from the d orbital of the Mn atom to the π* orbital of NO; the other is the π coordination bond, from the π* orbital of NO to the d orbital of the Mn atom. Since the Mn nitrosyls correspond to Mn^{II} oxidation state and d^5 electronic configuration, three types of Mn−NO bonds are possible to identify through NBO analysis. The σ coordination bond is relatively weak because it mainly arises from N lone pair electrons whereas having little contribution from the d_{z^2} orbital of Mn (see the Supporting Information, Figure S1). As shown from the orbital interaction diagrams of **b** and **d** in Figure 3, for **b**, the third occupied molecular orbital (HOMO-3) is formed by the highest-occupied fragment orbital (HOFO) and lowest-unoccupied fragment orbital (LUFO) of the [Mn(PaPy$_2$Q)] fragment (*f*1) and LUFO of the NO fragment (*f*2). The HOMO-3 is a π back-donating bond orbital with 0.041 e^- transfer from the d_{yz} orbital of the Mn atom to the π* orbital of NO. The π coordination bond orbital (HOMO−1) is formed by the interaction between the HOFO, LUFO, HOFO-2, and HOFO-3 of the *f*1 fragment and the HOFO of the *f*2 fragment, in which 0.036 e^- transfer from the π* orbital of NO to the d_{xz} orbital of the Mn atom. The lower energy and greater electron transfer of the π back-donating bond than that of π coordination bond indicate that the interaction of the π back-donating bond is stronger than that of the π coordination bond. In contrast, for **d**, the corresponding π back-donating bond orbital (HOMO−1) arises from the interaction between the

dx.doi.org/10.1021/ic2011953 | Inorg. Chem. 2012, 51, 3972−3980

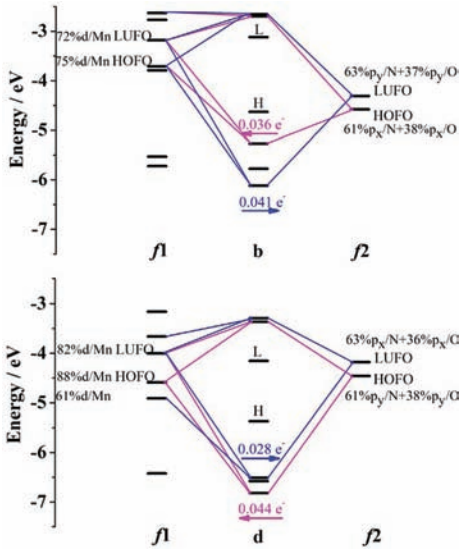

Figure 3. Orbital interaction diagrams obtained by TDDFT with the solvent of acetonitrile for **b** and **d**. *f*1 and *f*2 are interacting fragments.

LUFO, HOFO-1 of the *f*1, and LUFO of the *f*2 with 0.028 e^- transfer from the d_{xz} orbital of the Mn atom to the π^* orbital of NO, while the π coordination bond orbital (HOMO-3) arises from the interaction between the HOFO, LUFO of the *f*1, and HOFO of the *f*2 with 0.044 e^- transfer from the π^* orbital of NO to the d_{yz} orbital of the Mn atom. Therefore, according to the amount of electron transfer, the intensity of the π back-donating bond of **d** is much weaker than **b**, whereas the intensity of the π coordination bond of **d** is stronger than **b**.

To deeply explore the origin of the Mn−NO bond, take **d** for example, Wiberg's bond order analysis was performed.[52,53] Since Mn and NO atoms are placed on the *z* axis, their d_{z^2} orbital is responsible for the σ bond, d_{xz} and d_{yz} for the π bond, and d_{xy} and $d_{x^2-y^2}$ for the δ bond. Among these, the π bond is derived from d_{yz}(Mn)−p_y(N) and d_{xz}(Mn)−p_x(N). The Mn−N−O bond angle for **d** is 172.2°, which is nearly linear. Thus, according to eqs 1−3, the Mn−NO bond order is 1.45, where its subterms W_σ = 0.44, W_π = 0.91 ($W_{\pi x}$ = 0.44 and $W_{\pi y}$ = 0.47), and W_δ = 0.04. In addition, a similar trend was reported for the contribution analysis on the Mn−NO bond of $[Mn(CN)_5(NO)]^{3-}$ (28%W_σ, 72%W_π) complex in the work.[54] Apparently, the results of Wiberg's bond order show that the major contribution is π bond (63%), followed by σ bond (30%), to the Mn−NO covalent bond for **d**, which agrees well with the CDA results.

3.4. Molecular Orbital in Ground State. Most of studies[24,32,37,55,56] confirmed that the photodissociation of the metal complexes occurs with the antibonding orbital between metal and ligand. In addition, by analyzing the frontier molecular orbitals (FMOs), we can gain a better insight into the electronic structures of the complexes. The contour plots and energies levels of the most prominent FMOs involved in the electron transitions and the photolysis of orbital transitions for **a**−**d** are shown in Figure 4. As can be seen from Figure 4, the lowest unoccupied molecular orbital (LUMO) level of **b** is significantly lower than that of **a**, because of extended conjugation of the quinoline group in **b**. A similar situation is presented in **c** and **d**. However, the HOMO level is almost unchanged. These results suggest that the quinoline substitution remarkably influences the LUMO level of **b** and **d**.

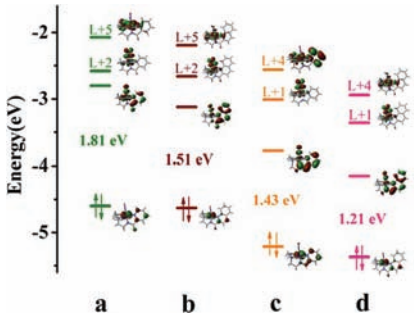

Figure 4. Calculated HOMO/LUMO energy diagrams are obtained by TDDFT with the solvent of acetonitrile of **a**−**d**, with energy gaps labeled. The most prominent MOs involved in the electron transitions and the photolysis of orbital transitions are also shown.

Complexes **c** and **d** with an imine group possess significantly lower HOMO and LUMO levels compared with those of carboxamide-substituted **a** and **b** due to the electron-accepting properties of the imine group. The calculated energy gaps of **a**−**d** are 1.81, 1.51, 1.43, and 1.21 eV, respectively. Therefore, the energy gaps are reduced by introducing the imine group and the quinoline group.

The FMO energies for **a**−**d**, along with their compositions, are listed in Table 3. The HOMOs of **a**−**d** are similar and mainly localized on metal d orbitals, with the contributions from d(Mn) orbitals of 83.4, 84.9, 83.1, and 80.4%, respectively. However, there exist noticeable differences in the LUMOs of **a**−**d**. In the case of **a** and **c**, the LUMO mainly originates from the π^* orbital of the NO and pyridine moieties, while for **b** and **d**, the π^* orbital of quinoline moiety predominantly contributes to the LUMO. Therefore, the changes of the ligands from **a** to **d** have a great effect on electron density distribution in the LUMO orbital, whereas little influence on the HOMO orbital. From Table 3 and Figure 4, we found that the LUMO+2 of **a** and **b** and the LUMO+1 and LUMO+2 of **c** and **d** have antibonding character between d_{yz}/d_{xz}(Mn) and π^*(NO) orbitals. Thus we may deduce that the LUMO+2 of **a** and **b** and the LUMO+1 or LUMO+2 of **c** and **d** should play a leading role in the photodissociation mechanism of the NO ligand.

3.5. Excited States. Since the light-induced ligand dissociation process is closely related to the excited states, the investigation on the transition character of the singlet and triplet excited states for **a**−**d** was carried out in our work. The character of each excited state is assigned as metal-to-ligand charge transfer (MLCT), ligand-to-ligand charge transfer (LLCT), ligand-to-metal charge transfer (LMCT), and metal center (MC), on the basis of the molecular orbital components analysis. In addition, many studies have shown that the metal nitrosyls release NO attributing to the electron transfer from d(M) orbitals to π^*(M−N) orbitals.[55−58] Among these, the photoactivity of the $\{Fe\text{-}NO\}^6$ nitrosyls and the $\{Ru\text{-}NO\}^6$ nitrosyls was attributed to electron transition from d_π(Fe) and d_π(Ru) orbitals to π^*(Fe−NO) and π^*(Ru−NO) orbitals by Greene et al. and Fry et al.,[55,56] respectively. Therefore, we presume that the photodissociation of $\{Mn\text{-}NO\}^6$ nitrosyls was regarded as undergoing a similar mechanism of releasing NO with those Fe and Ru nitrosyls but a unique photophysical and photochemical process. The real mechanism would give a detailed explanation, as seen below.

Herein, TD-BP86/TZVP,6-31g* simulated absorption spectra of **a**−**d** in acetonitrile are displayed in Figure 5. The detailed

dx.doi.org/10.1021/ic2011953 | *Inorg. Chem.* 2012, 51, 3972−3980

Table 3. Molecular Orbital Energies and Components (%) Obtained by TDDFT with the Solvent of Acetonitrile for a–d

	orbital	energy (eV)	MO composition (%)
a	LUMO+8	−1.83	31.5 π^* (pyridine) + 61.3 π^* (pyridyl-methyl)
	LUMO+7	−2.01	52.1 π^* (pyridine) + 36.9 π^* (pyridyl-methyl)
	LUMO+6	−2.03	20.6 $d_{x^2-y^2}$ (Mn) + 74.6 π^* (pyridyl-methyl)
	LUMO+5	−2.07	44.9 $d_{x^2-y^2}$ (Mn) + 42.8 π^* (pyridyl-methyl)
	LUMO+4	−2.32	27.9 d_{xz} (Mn) + 21.2 π^* (NO) + 41.0 π^* (pyridyl-methyl)
	LUMO+3	−2.39	45.1 π^* (pyridine) + 38.2 π^* (pyridyl-methyl)
	LUMO+2	−2.58	37.0 d_{yz} (Mn) + 57.1 π^* (NO)
	LUMO+1	−2.63	94.8 π^* (pyridyl-methyl)
	LUMO	−2.80	12.4 d_{xz} (Mn) + 30.8 π^* (NO) + 28.2 π^* (pyridine)
	HOMO	−4.60	83.4 d_{xy} (Mn)
	HOMO−1	−5.23	17.8 d_{yz} (Mn) + 19.1 π^* (NO) + 51.8 π^* (carboxamido-N)
b	LUMO+8	−1.85	60.0 π^* (pyridyl-methyl) + 29.8 π^* (quinoline)
	LUMO+7	−2.01	48.6 π^* (pyridyl-methyl) + 43.0 π^* (quinoline)
	LUMO+6	−2.05	87.8 π^* (pyridyl-methyl)
	LUMO + 5	−2.19	65.7 $d_{x^2-y^2}$ (Mn)+15.2 π^* (pyridyl-methyl)
	LUMO+4	−2.36	18.8 d_{yz} (Mn) + 71.1 π^* (pyridyl-methyl)
	LUMO+3	−2.57	18.4 π^* (NO) + 49.2 π^* (pyridyl-methyl)
	LUMO+2	−2.66	35.3 d $_{xz}$ (Mn) + 48.8 π^* (NO)
	LUMO+1	−2.70	13.2 d_{yz} (Mn) + 25.4 π^* (NO) + 45.5 π^* (pyridyl-methyl)
	LUMO	−3.12	6.9 d_{xy} (Mn) + 9.7 π^* (NO) + 68.5 π^* (quinoline)
	HOMO	−4.63	84.9 d_{xy} (Mn)
	HOMO−1	−5.27	16.2 d_{yz} (Mn) + 19.1 π^* (NO) + 52.4 π^* (carboxamido-N)
c	LUMO+7	−2.20	51.9 d_{z^2} (Mn) + 36.9 π^* (pyridyl-methyl)
	LUMO+6	−2.44	10.0 d_{xz} (Mn) + 62.8 π^* (pyridyl-methyl) + 25.2 π^* (pyridine)
	LUMO+5	−2.47	55.0 d_{z^2} (Mn) + 16.0 π^* (pyridyl-methyl) + 12.4 π^* (pyridine)
	LUMO+4	−2.56	12.1 $d_{x^2-y^2}$ (Mn) + 65.7 π^* (pyridine)
	LUMO+3	−2.75	89.9 π^* (pyridyl-methyl)
	LUMO+2	−2.92	28.0 d_{xz} (Mn) + 48.7 π^* (NO)
	LUMO+1	−3.01	35.0 d_{yz} (Mn) + 59.1 π^* (NO)
	LUMO	−3.78	8.3 d_{xz} (Mn) +13.3 π^* (NO) + 34.2 π^* (pyridine) + 37.0 π^* (imine)
	HOMO	−5.21	83.1 d_{xy} (Mn)
	HOMO−1	−6.38	50.0 d_{xz} (Mn) + 21.3 π^* (NO) + 13.2 π^* (pyridyl-methyl)
d	LUMO+7	−2.57	48.6 d_{z^2} (Mn) + 9.4 π^* (NO) + 31.8 π^* (pyridyl-methyl)
	LUMO+6	−2.61	18.4 π^* (pyridyl-methyl) + 61.0 π^* (quinoline) + 11.8 π^* (imine)
	LUMO+5	−2.74	11.6 d_{yz} (Mn) + 70.0 π^* (pyridyl-methyl) + 13.0 π^* (quinoline)
	LUMO+4	−2.94	55.8 $d_{x^2-y^2}$ (Mn) + 26.2 π^* (pyridyl-methyl)
	LUMO+3	−2.99	21.3 d_{z^2} (Mn) + 64.7 π^* (pyridyl-methyl)
	LUMO+2	−3.29	27.9 d_{yz} (Mn) + 47.4 π^* (NO)
	LUMO+1	−3.36	37.7 d_{xz} (Mn) + 56.1 π^* (NO)
	LUMO	−4.15	8.8 d_{xy} (Mn) + 10.9 π^* (NO) + 42.7 π^* (quinoline) + 31.1 π^* (imine)
	HOMO	−5.37	80.4 d_{xy} (Mn)
	HOMO−1	−6.51	43.7 d_{yz} (Mn) + 26.3 π^* (NO) + 12.0 π^* (pyridyl-methyl) + 12.3 π^* (quinoline)
	HOMO−2	−6.58	91.0 π^* (quinoline)

information, such as excitation energies, oscillator strengths (f), dominant configurations (with larger CI coefficients), and transitions character of **a**–**d** in acetonitrile are listed in Table 4.

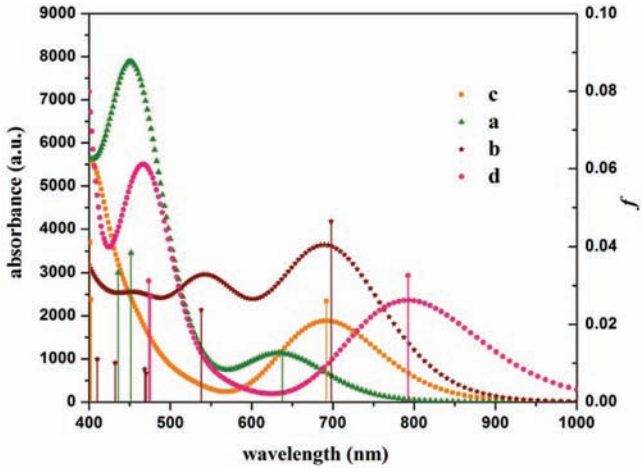

Figure 5. Simulated absorption spectra for complexes in MeCN: $[Mn(PaPy_3)(NO)]^+$ (**a**), $[Mn(PaPy_2Q)(NO)]^+$ (**b**), $[Mn(SBPy_3)(NO)]^{2+}$ (**c**), $[Mn(SBPy_2Q)(NO)]^{2+}$ (**d**).

As can be seen from Figure 5, the absorption spectra of **a**–**d** exhibit two bands. By comparing the experimental and theoretical results, we found that the low-energy band corresponds to the lowest singlet excited state (S_1) for **a**–**d**, consistent with the experiment results. The S_1 is ascribed to the HOMO to LUMO transition, with an absorption wavelength of 638, 698, 692, and 792 nm, respectively. The absorption wavelength shows a significant red shift from **a** to **d**, which is in accordance with the trend of the calculated HOMO–LUMO energy gap from **a** to **d**. The transition character for the absorption is ascribed to an MLCT state. In **a** and **b**, the transition occurs from the d_{xy} orbitals of Mn to the d_{xz}/d_{xy} orbitals of Mn and the π^* orbitals of NO and pyridine/quinoline, whereas for **c** and **d**, the transition occurs from the d_{xy} orbitals of Mn to the d_{xz}/d_{xy} orbitals of Mn and the π^* orbitals of NO, imine, and pyridine/quinoline. However, from Table 4 and Figure 5, we found that the deviation between the calculated and the experimental high-energy bands becomes noticeable. Especially for **b**, the absorption strength and wavelength were inconsistent with the experiment data. Most importantly, the absorption of **d** was confirmed to be in the NIR region by experiments and theoretical calculation, suggesting that **d** could be more suitable as a candidate for PDT than the others. Thus, our research on the mechanism of NO photorelease has been focused on the low-energy region. It should be noted that, on the basis of the above analysis and electron transition results (Table 4), all the singlet excited states of **a**–**d** are not involved in the antibonding character between d_{yz}/d_{xz} (Mn) orbitals and π^*(NO) orbitals of LUMO +2 in **a** and **b** as well as LUMO+1 or LUMO+2 in **c** and **d**. Thus, we could predict that the photodissociation of **a**–**d** has little probability under the singlet excited states.

To further investigate the probability of photodissociation in triplet excited states, we also analyzed the transition nature into the T_1 and T_2 states. The detailed results are collected in Table 4. Notice that the T_1 states of **a**–**d** have similar transition nature with the S_1 states, mainly originating from HOMO → LUMO transition. So it is impossible for **a**–**d** to occur the photodissociation at the T_1 state. In contrast, the T_2 states of **a** and **b** are derived from HOMO → LUMO+2 and HOMO → LUMO+5 transitions with $[d_{xy}(Mn) \rightarrow \pi^*(Mn-N_6) + d_{yz}/d_{xz}(Mn)]$ (MLCT/MC) and $[d_{xy}(Mn) \rightarrow d_{x^2-y^2}(Mn)]$ (MC)

dx.doi.org/10.1021/ic2011953 | Inorg. Chem. 2012, 51, 3972–3980

Table 4. Calculated Excited Energies, Dominant Orbital Excitation, and Oscillator Strength (f) by TDDFT with the Solvent of Acetonitrile for a−d

	state	composition	E(eV)	λ(nm)	f	character
		Singlet Excited States				
a	S_1	HOMO → LUMO (0.81)	1.94	638	0.013	MLCT
	S_{11}	HOMO−1 → LUMO (0.32)	2.74	452	0.038	MC/ LLCT
		HOMO−1 → LUMO +2 (0.22)				LMCT/ LLCT
	S_{12}	HOMO → LUMO+8 (0.58)	2.84	436	0.033	MLCT
b	S_1	HOMO → LUMO (0.89)	1.78	698	0.046	MLCT
	S_5	HOMO−1 → LUMO (0.80)	2.30	538	0.024	MC/ LLCT
	S_9	HOMO−1 → LUMO +1 (0.50)	2.64	470	0.007	LLCT
	S_{10}	HOMO → LUMO+7 (0.89)	2.65	469	0.008	MLCT
	S_{14}	HOMO−1 → LUMO +3 (0.41)	2.87	432	0.010	MLCT/ LLCT
	S_{15}	HOMO−1 → LUMO +4 (0.41)	3.02	410	0.011	LLCT
c	S_1	HOMO → LUMO (0.94)	1.79	692	0.026	MLCT
	S_9	HOMO → LUMO+6 (0.31)	3.08	403	0.026	MC/ MLCT
	S_{10}	HOMO → LUMO+7 (0.48)	3.09	402	0.041	MC/ MLCT
d	S_1	HOMO → LUMO (0.96)	1.56	792	0.033	MLCT
	S_6	HOMO−2 → LUMO (0.71)	2.61	475	0.027	LMCT/ LLCT
	S_7	HOMO−1 → LUMO (0.58)	2.62	474	0.031	MLCT/ LLCT
		Triplet Excited States				
a	T_1	HOMO → LUMO (0.86)	1.59	780		MLCT
	T_2	HOMO → LUMO+2 (0.66)	1.64	757		MC/ MLCT
		HOMO → LUMO+5 (0.25)				MC/ MLCT
b	T_1	HOMO → LUMO (0.94)	1.30	952		MLCT
	T_2	HOMO → LUMO+5 (0.46)	1.52	814		MC/ MLCT
		HOMO → LUMO+2 (0.43)				MC/ MLCT
c	T_1	HOMO → LUMO (0.67)	1.16	1071		MLCT
	T_2	HOMO → LUMO+1 (0.67)	1.77	702		MC/ MLCT
		HOMO → LUMO+4 (0.30)				MC/ MLCT
d	T_1	HOMO → LUMO (0.99)	0.96	1295		MLCT
	T_2	HOMO → LUMO+4 (0.44)	1.60	774		MC/ MLCT
		HOMO → LUMO+1 (0.42)				MC/ MLCT

characters. Both **c** and **d** are also involved in two types of transitions: HOMO → LUMO+1 and HOMO → LUMO+4. The HOMO → LUMO+1 transition of **c** and **d** is characterized as [d_{xy}(Mn) → π^*(Mn−N_6) + d_{yz}/d_{xz}(Mn)] (MLCT/MC). The HOMO → LUMO+4 transition of **c** is characterized as [d_{xy}(Mn) → π^*(Mn−N_6) + π^*(pyridine)] (MLCT); whereas **d** is characterized as [d_{xy}(Mn) → $d_{x^2-y^2}$(Mn)] (MC). Finally, based on orbital components analysis (Table 3) and electron transition results (Table 4) mentioned above, we know that only the T_2 state is mainly involved in antibonding orbital transition: HOMO → LUMO+2 in **a** and **b** and HOMO → LUMO+1 in **c** and **d**. Therefore, we could predict that the T_2 state plays an important role in the photodissociation process of **a**−**d**.

3.6. Mechanism of Photodissociation. To prove the probability of photodissociation in the T_2 state, we investigated the energy separations between S_1 and T_n states ($E(S_1 \rightarrow T_n)$), and between T_n and T_1 states ($E(T_n \rightarrow T_1)$), since the intersystem crossing (ISC) and internal conversion (IC) abilities were qualitatively described through investigation of the S_1−T_n and T_n−T_1 energy separation.[59,60] It should be noted that the smaller $E(S_1 \rightarrow T_n)$ is, the faster the ISC rate; whereas the larger $E(T_n \rightarrow T_1)$ is, the slower the IC rate.[61,62] Thus, take **d** for example, we found from Figure 6, that the

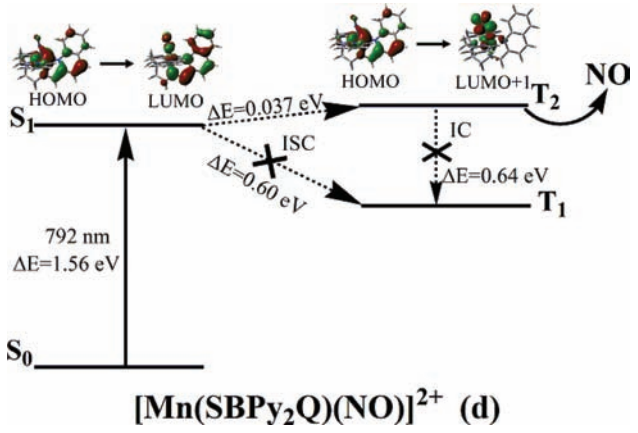

Figure 6. Photodissociation of dominant transition states for **d**.

$E(S_1 \rightarrow T_2)$ is small (0.037 eV) with different configurations, indicating an effective ISC may occur from S_1 to T_2 states. In addition, since the $E(T_2 \rightarrow T_1)$ is relatively large (0.64 eV), it is efficient to suppress the IC between them, which suggests that the excited state may have enough time to remain at the T_2 state.

Many theoretical works investigated the mechanism of ligand dissociation based on PECs of difference states.[30,63−65] In order to give enough evidence for the photodissociation for Mn nitrosyls occurring at the T_2 state, we also investigated the PECs of **d** with the Mn−N_6 bond distance elongated in the S_0, S_{0mix}, S_1, T_1, and T_2 states. From Figure 7a, we know when the Mn−N_6 bond length is 1.86 Å, the energies of T_1(TDDFT) and T_1(UKS) states are same and only three points of PECs were obtained by T_1(TDDFT). Therefore, we inferred the release of NO might occur at the Mn−N_6 bond length that is larger than 1.86 Å. Then, as the Mn−N_6 bond length is elongated from 1.86 Å, the energies of S_0, S_1, and T_1 states show an obvious increasing tendency, while the energy of T_2 state shows gently PEC. These analyses indicate $S_0 \rightarrow S_1 \rightarrow T_2 \rightarrow$ dissociation should be a rational route for the Mn−N_6 bond photodissociation process. According to the assignments of respective excited states, three other complexes would undergo similar photodissociation processes.

Then, the EDDMs of the T_2 state further illustrate that the photodissociation of **d** is shown in Figure 7b. As seen in Figure 7b, the minimum energy of PEC at the T_2 state (whose character was traced by EDDM) of **d** was found with the Mn−

dx.doi.org/10.1021/ic2011953 | Inorg. Chem. 2012, 51, 3972−3980

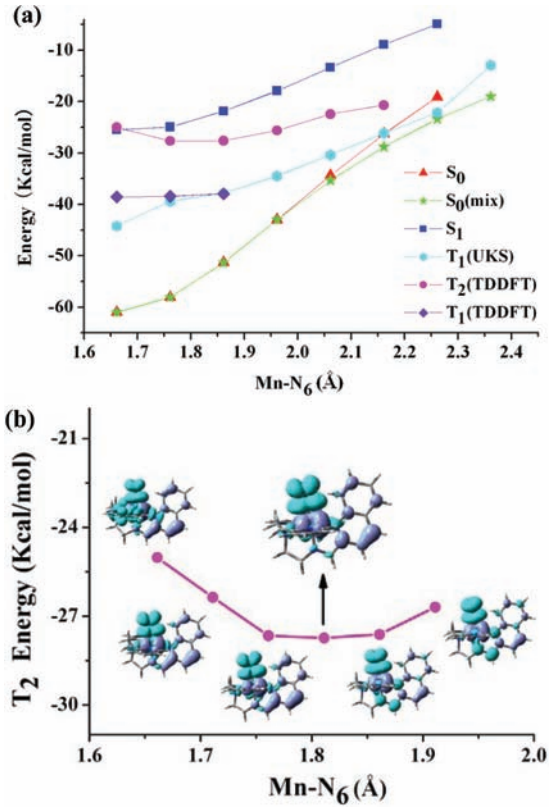

Figure 7. (a) PECs of **d** at difference states, along the Mn−N_6 bond stretch calculated at different levels. (b) PEC of the T_2 state of **d** along the Mn−N_6 coordinates. Selected EDDMs are presented in order to show the change in character of the T_2 state. The zero-point of the energy scale is set to the S_0 energy at its equilibrium geometry.

N_6 bond at 1.81 Å, suggesting that the photodissociation has to overcome a small energy barrier and then release NO. In addition, when the Mn−N_6 bond length is 1.86 Å, the character of the T_2 state is changed from the admixture of MLCT and MC states to the admixture of MLCT, MC, and LLCT states. It is clearly proven that this state is not the original T_2 state, thus the photorelease of NO has occurred.

In order to qualitatively explain the ability of releasing NO from the complexes, we calculated the $E(S_1 \rightarrow T_2)$ and the $E(T_2 \rightarrow T_1)$. We know that the ability of releasing NO from the complexes may be strong if the $E(S_1 \rightarrow T_2)$ is small and the $E(T_2 \rightarrow T_1)$ is large. From Figure 8, for **a**−**c**, the T_2 energy is lower than that of S_1, and the $E(S_1 \rightarrow T_2)$ is 0.31, 0.25, and 0.02 eV, respectively, so the ability of ISC $(S_1 \rightarrow T_2)$ may gradually

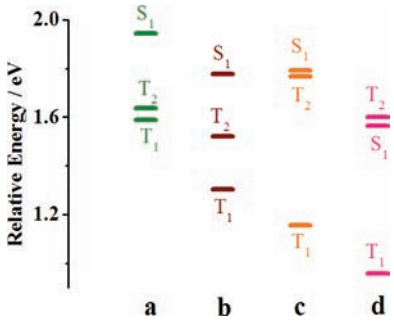

Figure 8. Calculated relative energy levels in the S_1 state conformation of **a**−**d**.

increase from **a** to **c**. However, for **d**, even though the energy of T_2 is higher than that of S_1, the ISC from S_1 to T_2 might be easily achieve, since the $E(S_1 \rightarrow T_2)$ (0.04 eV) is very small. It is worthwhile to note that the $E(T_2 \rightarrow T_1)$ of **a** is small, so the IC from T_2 to T_1 might be fast, thus the possibility of the photorelease of NO from **a** may be small at the NIR region. However, for **b**−**d**, as the $E(T_2 \rightarrow T_1)$ gradually increases, the ability of IC from T_2 to T_1 may gradually weaken. Therefore, the ability of the photorelease of NO from **b**−**d** may gradually strengthen in the NIR region.

4. CONCLUSIONS

We investigated the electronic structures and optoelectronic properties of the four Mn(II) complexes coordinated with schiff base or carbonyl amine ligands. It was found that the electronic properties of the amine and quinoline ligands have a great influence on the photophysical properties of complexes, such as energy gaps and absorption spectra. The decrease of energy gaps was attributed to the increase of conjugation and the introduction of an electron-withdrawing ligand. Since the maximum absorption wavelength of **d** was obtained in the NIR region by experiments and theoretical calculation, the photorelease of NO could be achieved in the NIR region, which is favorable for its application in the medical field. In addition, the J_{ab} value and the spin density distribution of **d** confirmed that **d** possesses the diamagnetic at the ground state.

By the NBO, CDA, and Wiberg's bond order analysis, the Mn−N_6 bond has three bonding modes: σ coordination, π back-donating, and π coordination. Moreover, the contribution to the Mn−N_6 bond mainly originates from the π bond. On the basis of the orbital component analysis, we deduce that the LUMO+2 of **a** and **b** and the LUMO+1 or LUMO+2 of **c** and **d** with the antibonding character between d_{yz}/d_{xz}(Mn) and π^*(NO) orbitals should play a leading role in the photodissociation mechanism of the NO ligand. Furthermore, the T_2 state is responsible for the photorelease of NO, whereas the singlet excited states and the T_1 state are not involved in the photodissociation of the NO ligand by analyzing the electron transition property. Then, the PECs and EDDMs provide enough evidence that the Mn−N_6(O_1) bond photodissociation process occurs at the T_2 state. Therefore, a reasonable scenario for the photodissociation pathway can be described as $S_0 \rightarrow S_1 \rightarrow T_2 \rightarrow$ dissociation, i.e., absorption of a photon to the singlet excited state, followed by the ISC from S_1 to T_2, and the IC from T_2 with the photodissociation occurrence.

■ ASSOCIATED CONTENT

Ⓢ Supporting Information

Cartesian coordinates of the four complexes studied from BP86-optimized geometries and orbital interaction diagram for **b** and **d**. This material is available free of charge via the Internet at http://pubs.acs.org.

■ AUTHOR INFORMATION

Corresponding Author

*E-mail: zmsu@nenu.edu.cn.

Notes

The authors declare no competing financial interest.

■ ACKNOWLEDGMENTS

The authors gratefully acknowledge financial support from NSFC (20903020 and 21131001), 973 Program

(2009CB623605), SRF for ROCS, SEM, and the Science and Technology Development Planning of Jilin Province (20090146).

REFERENCES

(1) Palmer, R. M. J.; Ferrige, A. G.; Moncada, S. *Nature* **1987**, *327*, 524−526.
(2) Ignarro, L. J.; Buga, G. M.; Wood, K. S.; Byrns, R. E.; Chaudhuri, G. *Proc. Natl. Acad. Sci. U.S.A.* **1987**, *84*, 9265−9269.
(3) Culotta, E.; Koshland, D. E. Jr *Science* **1992**, *258*, 1862−1865.
(4) Ignarro, L. J. *Angew. Chem., Int. Ed.* **1999**, *38*, 1882−1892.
(5) Murad, F. *Angew. Chem., Int. Ed.* **1999**, *38*, 1856−1868.
(6) Furchgott, R. F. *Angew. Chem., Int. Ed.* **1999**, *38*, 1870−1880.
(7) Kalsner, S. *Nitric oxide and free radicals in peripheral neurotransmission*; Birkhauser: Boston, 2000.
(8) Lincoln, J.; Hoyle, C.; Burnstock, G. *Nitric oxide in health and disease*; Cambridge Univ Press: New York, 1997.
(9) Elphick, M. *J. Neurochem.* **1996**, *67*, 438.
(10) McCleverty, J. A. *Chem. Rev.* **2004**, *104*, 403−418.
(11) Ford, P. C.; Bourassa, J.; Miranda, K.; Lee, B.; Lorkovic, I.; Boggs, S.; Kudo, S.; Laverman, L. *Coord. Chem. Rev.* **1998**, *171*, 185−202.
(12) Ford, P. C.; Laverman, L. E. *Coord. Chem. Rev.* **2005**, *249*, 391−403.
(13) Rose, M. J.; Mascharak, P. K. *Coord. Chem. Rev.* **2008**, *252*, 2093−2114.
(14) Prakash, R.; Czaja, A. U.; Heinemann, F. W.; Sellmann, D. *J. Am. Chem. Soc.* **2005**, *127*, 13758−13759.
(15) De Candia, A. G.; Marcolongo, J. P.; Etchenique, R.; Slep, L. D. *Inorg. Chem.* **2010**, *49*, 6925−6930.
(16) Conrado, C. L.; Bourassa, J. L.; Egler, C.; Wecksler, S.; Ford, P. C. *Inorg. Chem.* **2003**, *42*, 2288−2293.
(17) Wecksler, S.; Mikhailovsky, A.; Ford, P. C. *J. Am. Chem. Soc.* **2004**, *126*, 13566−13567.
(18) Wecksler, S. R.; Mikhailovsky, A.; Korystov, D.; Ford, P. C. *J. Am. Chem. Soc.* **2006**, *128*, 3831−3837.
(19) Sauaia, M. G.; de Lima, R. G.; Tedesco, A. C.; da Silva, R. S. *J. Am. Chem. Soc.* **2003**, *125*, 14718−14719.
(20) Eroy-Reveles, A. A.; Hoffman-Luca, C. G.; Mascharak, P. K. *Dalton Trans.* **2007**, 5268−5274.
(21) Rose, M. J.; Olmstead, M. M.; Mascharak, P. K. *J. Am. Chem. Soc.* **2007**, *129*, 5342−5343.
(22) Fry, N. L.; Heilman, B. J.; Mascharak, P. K. *Inorg. Chem.* **2010**, *50*, 317−324.
(23) Ghosh, K.; Eroy-Reveles, A. A.; Avila, B.; Holman, T. R.; Olmstead, M. M.; Mascharak, P. K. *Inorg. Chem.* **2004**, *43*, 2988−2997.
(24) Eroy-Reveles, A. A.; Leung, Y.; Beavers, C. M.; Olmstead, M. M.; Mascharak, P. K. *J. Am. Chem. Soc.* **2008**, *130*, 4447−4458.
(25) Hoffman-Luca, C. G.; Eroy-Reveles, A. A.; Alvarenga, J.; Mascharak, P. K. *Inorg. Chem.* **2009**, *48*, 9104−9111.
(26) Merkle, A. C.; Fry, N. L.; Mascharak, P. K.; Lehnert, N. *Inorg. Chem.* **2011**, *50*, 12192−12203.
(27) Carreón-Macedo, J.-L.; Harvey, J. N. *J. Am. Chem. Soc.* **2004**, *126*, 5789−5797.
(28) Goossen, L. J.; Koley, D.; Hermann, H. L.; Thiel, W. *J. Am. Chem. Soc.* **2005**, *127*, 11102−11114.
(29) Kuta, J.; Patchkovskii, S.; Zgierski, M. Z.; Kozlowski, P. M. *J. Comput. Chem.* **2006**, *27*, 1429−1437.
(30) Jaworska, M.; Lodowski, P.; Andruniów, T.; Kozlowski, P. M. *J. Phys. Chem. B* **2007**, *111*, 2419−2422.
(31) Bühl, M.; Kabrede, H. *J. Chem. Theory Comput.* **2006**, *2*, 1282−1290.
(32) Lodowski, P.; Jaworska, M.; Andruniów, T.; Kumar, M.; Kozlowski, P. M. *J. Phys. Chem. B* **2009**, *113*, 6898−6909.
(33) Tong, G. S. M.; Wong, E. L.-M.; Che, C.-M. *Chem.−Eur. J.* **2008**, *14*, 5495−5506.
(34) DeBeer George, S.; Petrenko, T.; Neese, F. *J. Phys. Chem. A* **2008**, *112*, 12936−12943.
(35) Becke, A. D. *Phys. Rev. A* **1988**, *38*, 3098−3100.
(36) Perdew, J. P. *Phys. Rev. B* **1986**, *33*, 8822−8824.
(37) Praneeth, V. K. K.; Paulat, F.; Berto, T. C.; George, S. D.; Näther, C.; Sulok, C. D.; Lehnert, N. *J. Am. Chem. Soc.* **2008**, *130*,, 15288−15303.
(38) Barone, V.; Cossi, M.; Tomasi, J. *J. Chem. Phys.* **1997**, *107*, 3210−3221.
(39) Reed, A. E.; Curtiss, L. A.; Weinhold, F. *Chem. Rev.* **1988**, *88*, 899−926.
(40) Dapprich, S.; Frenking, G. *J. Phys. Chem.* **1995**, *99*, 9352−9362.
(41) Rusanova, J.; Rusanov, E.; Gorelsky, S. I.; Christendat, D.; Popescu, R.; Farah, A. A.; Beaulac, R.; Reber, C.; Lever, A. B. P. *Inorg. Chem.* **2006**, *45*, 6246−6262.
(42) Gorelsky, S. I. *AOMix: Program for Molecular Orbital Analysis*; University of Ottawa, 2010; http://www.sg-chem.net/.
(43) Gorelsky, S. I.; Lever, A. B. P. *J. Organomet. Chem.* **2001**, *635*, 187−196.
(44) O'Boyle, N. M.; Tenderholt, A. L.; Langner, K. M. *J. Comput. Chem.* **2008**, *29*, 839−845.
(45) Reed, A. E.; Weinstock, R. B.; Weinhold, F. *J. Chem. Phys.* **1985**, *83*, 735−746.
(46) Nagao, H.; Nishino, M.; Shigeta, Y.; Soda, T.; Kitagawa, Y.; Onishi, T.; Yoshioka, Y.; Yamaguchi, K. *Coord. Chem. Rev.* **2000**, *198*, 265−295.
(47) Noodleman, L.; Case, D. A.; Aizman, A. *J. Am. Chem. Soc.* **1988**, *110*, 1001−1005.
(48) Frisch, M. J.; Trucks, G. W.; Schlegel, H. B.; Scuseria, G. E.; Robb, M. A.; Cheeseman, J. R.; Scalmani, G.; Barone, V.; Mennucci, B.; Petersson, G. A.; Nakatsuji, H.; Caricato, M.; Li, X.; Hratchian, H. P.; Izmaylov, A. F.; Bloino, J.; Zheng, G.; Sonnenberg, J. L.; Hada, M.; Ehara, M.; Toyota, K.; Fukuda, R.; Hasegawa, J.; Ishida, M.; Nakajima, T.; Honda, Y.; Kitao, O.; Nakai, H.; Vreven, T.; Montgomery, J. A., Jr.; Peralta, J. E.; Ogliaro, F.; Bearpark, M.; Heyd, J. J.; Brothers, E.; Kudin, K. N.; Staroverov, V. N.; Kobayashi, R.; Normand, J.; Raghavachari, K.; Rendell, A.; Burant, J. C.; Iyengar, S. S.; Tomasi, J.; Cossi, M.; Rega, N.; Millam, J. M.; Klene, M.; Knox, J. E.; Cross, J. B.; Bakken, V.; Adamo, C.; Jaramillo, J.; Gomperts, R.; Stratmann, R. E.; Yazyev, O.; Austin, A. J.; Cammi, R.; Pomelli, C.; Ochterski, J. W.; Martin, R. L.; Morokuma, K.; Zakrzewski, V. G.; Voth, G. A.; Salvador, P.; Dannenberg, J. J.; Dapprich, S.; Daniels, A. D.; Farkas, O.; Foresman, J. B.; Ortiz, J. V.; Cioslowski, J.; Fox, D. J. *Gaussian 09*, revision A.02 [P]; Gaussian, Inc.: Wallingford, CT, 2009.
(49) Shi, L. L.; Hong, B.; Guan, W.; Wu, Z. J.; Su, Z. M. *J. Phys. Chem. A* **2010**, *114*, 6559−6564.
(50) Takano, Y.; Taniguchi, T.; Isobe, H.; Kubo, T.; Morita, Y.; Yamamoto, K.; Nakasuji, K.; Takui, T.; Yamaguchi, K. *J. Am. Chem. Soc.* **2002**, *124*, 11122−11130.
(51) Ni, Z.; Ren, X.; Ma, J.; Xie, J.; Ni, C.; Chen, Z.; Meng, Q. *J. Am. Chem. Soc.* **2005**, *127*, 14330−14338.
(52) Sizova, O. V.; Sokolov, A. Y.; Skripnikov, L. V.; Baranovski, V. I. *Polyhedron* **2007**, *26*, 4680−4690.
(53) Sizova, O. V.; Skripnikov, L. V.; Sokolov, A. Y.; Sizov, V. V. *Int. J. Quantum Chem.* **2009**, *109*, 2581−2590.
(54) Li, Q.; Gao, D.; Yin, J.; Li, S. *J. Mol. Struct.: THEOCHEM* **2008**, *865*, 88−93.
(55) Greene, S. N.; Richards, N. G. J. *Inorg. Chem.* **2004**, *43*, 7030−7041.
(56) Fry, N. L.; Rose, M. J.; Rogow, D. L.; Nyitray, C.; Kaur, M.; Mascharak, P. K. *Inorg. Chem.* **2010**, *49*, 1487−1495.
(57) Works, C. F.; Jocher, C. J.; Bart, G. D.; Bu, X.; Ford, P. C. *Inorg. Chem.* **2002**, *41*, 3728−3739.
(58) Gorelsky, S. I.; Lever, A. B. P. *Int. J. Quantum Chem.* **2000**, *80*, 636−645.
(59) Kleinschmidt, M.; Tatchen, J.; Marian, C. M. *J. Comput. Chem.* **2002**, *23*, 824−833.
(60) Burin, A. L.; Ratner, M. A. *J. Chem. Phys.* **1998**, *109*, 6092−6102.
(61) Shi, L. L.; Li, T.; Zhao, S. S.; Li, H.; Su, Z. M. *Theor. Chem. Acc.* **2009**, *124*, 29−36.

(62) Turro, N. J. *Modern Molecular Photochemistry*; University Science Books: Mill Valley, 1991.
(63) Dreuw, A.; Dunietz, B. D.; Head-Gordon, M. *J. Am. Chem. Soc.* **2002**, *124*, 12070−12071.
(64) Goumans, T. P. M; Ehlers, A. W.; van Hemert, M. C.; Rosa, A.; Baerends, E.-J.; Lammertsma, K. *J. Am. Chem. Soc.* **2003**, *125*, 3558−3567.
(65) Dunietz, B. D.; Dreuw, A.; Head-Gordon, M. *J. Phys. Chem. B* **2003**, *107*, 5623−5629.